Development of the High-Pressure Electro-Dynamic Gradient Crystal-Growth Technology for Semi-Insulating CdZnTe Growth for Radiation Detector Applications

CSABA SZELES,[1,2] SCOTT E. CAMERON,[1] STEPHEN A. SOLDNER,[1] JEAN-OLIVIER NDAP,[1] and MICHAEL D. REED[1]

1.—eV PRODUCTS, a division of II-VI, Inc., Saxonburg, PA 16056. 2.—cszeles@II-VI.com

The high-pressure electro-dynamic gradient (HP-EDG) crystal-growth technology has been recently developed and introduced at eV PRODUCTS to grow large-volume, semi-insulating (SI) CdZnTe single crystals for room-temperature x-ray and gamma-ray detector applications. The new HP growth technology significantly improves the downstream CdZnTe device-fabrication yield compared to earlier versions of the HP crystal-growth technology because of the improved structural and charge-transport properties of the CdZnTe ingots. The new state-of-the-art, HP-EDG crystal-growth systems offer exceptional flexibility and thermal and mechanical stability and allow the growth of high-purity CdZnTe ingots. The flexibility of the multi-zone heater system allows the dynamic control of heat flow to optimize the growth-interface shape during crystallization. This flexibility combined with an advanced control system, improved system diagnostics, and realistic heat-transport modeling provides an excellent platform for continuing process development. Initial results on large-diameter (140 mm), SI $Cd_{1-x}Zn_xTe$ ($x = 0.1$) ingots grown in low temperature gradients with the HP-EDG technique show reduced defect density and complete elimination of ingot cracking. The increased single-crystal yield combined with the improved charge transport allows the fabrication of large-volume, high-sensitivity, high energy-resolution detector devices at increased yield. The CdZnTe ingots grown to date produced large-volume crystals (≥ 1 cm^3) with electron mobility-lifetime product ($\mu\tau_e$) in the $(3–7) \times 10^{-3}$ cm^2/V range. The lower-than-desired charge-transport uniformity of the HP-EDG CdZnTe ingots is associated with the high density of Te inclusions formed in the ingots during crystallization. The latest process-development efforts show a reduction in the Te-inclusion density, an increase of the charge-transport uniformity, and improved energy resolution of the large-volume detectors fabricated from these crystals.

Key words: Semi-insulating cadmium zinc telluride (CdZnTe), nuclear radiation detectors, electro-dynamic gradient (EDG) technique, x-ray and γ-ray spectroscopy

INTRODUCTION

The physical properties of semi-insulating (SI) cadmium zinc telluride (CdZnTe), such as high atomic number, high density, wide bandgap, low chemical reactivity, and long-term stability, make it an excellent material candidate for high-efficiency, high-resolution room-temperature nuclear-radiation detectors. Intense research on electrical compensation and defect formation in $Cd_{1-x}Zn_xTe$, $0 \leq \times \leq 1$, in the last 10–15 years led to the development of crystal-growth processes that allow the growth of fully compensated, SI CdZnTe crystals with low defect density and very good charge-transport properties.

(Received October 14, 2003; accepted November 21, 2003)

Few industrial companies around the world significantly contributed to this research and pioneered the commercialization of both CdTe and CdZnTe crystals. Today, SI CdZnTe crystals are available commercially, and the CdZnTe-based, room-temperature radiation detectors and detector arrays are steadily gaining acceptance in many medical, industrial, security, safeguards, and scientific x-ray and γ-ray imaging and spectroscopic applications.[1–3]

While CdZnTe crystals are readily available for simpler counting and monitoring applications, large field-of-view imaging and high-sensitivity, high-resolution spectroscopic applications continuously demand larger and larger and more and more uniform CdZnTe single crystals. The growth of SI CdZnTe crystals, with spatially uniform charge-transport properties that are required by these applications, poses a considerable challenge because of the inherent complexity of the crystallization and defect-formation processes in these II-VI compounds.[4,5]

Commercially available SI CdZnTe with charge-transport properties satisfactory for detector applications has been mostly grown by the high-pressure Bridgman (HPB)[6–9] or conventional horizontal-Bridgman[10] technique, while commercial SI CdTe is typically grown by the traveling-heater method.[11] Recently, growth with the conventional vertical-Bridgman approach has been also successfully introduced.[12,13] Most of the CdZnTe ingots are grown from melt containing 10% Zn. Because of Zn segregation, the Zn concentration varies along the growth direction of the ingot between 5% and 13%. The electrical resistivity of the crystals is in the $(1–4) \times 10^{10}$ Ωcm range. Such a high resistivity is achieved with some form of active electrical-compensation technique. Typically, good electron transport is reported with electron mobility-lifetime product in the $\mu\tau_e = (0.5–6) \times 10^{-3}$ cm^2/V range, while hole transport is typically found to be poor, $\mu\tau_h = (0.2–5) \times 10^{-5}$ cm^2/V (all measured at room temperature).

eV PRODUCTS (Saxonburg, PA) has been practicing the HPB growth of CdZnTe since 1992. Between 1992 and 1998, the process development team introduced two new, improved HPB crystal-growth systems and scaled up the growth from 3.5-in. (90 mm) diameter, 4-kg ingots to 5.5-in. (140 mm) diameter, 10-kg ingots. Between 1998 and 2000, the high-pressure gradient freeze (HPGF) technique was developed and introduced to production. The HPGF technique eliminates the motion of the crucible relative to the heater and reduces some of the heat-transport problems associated with HPB growth.[4] The HPGF technique improved the single-crystal yield and virtually eliminated the formation of pipes in the CdZnTe ingots. The HPGF-grown CdZnTe ingots, however, still suffered from cracking caused by excessive thermal stress during crystallization and cool down of the ingots. In 2000, eV PRODUCTS initiated the development of a multi-zone high-pressure electro-dynamic gradient (HP-EDG) crystal-growth system and process to reduce thermal stress in the CdZnTe ingots and eliminate ingot cracking and improve the downstream detector-device fabrication yield. In the EDG technique, the crucible and the heater are stationary, and the gradient is translated through the molten CdZnTe electronically.[14] The EDG technique avoids many of the inherent problems of the Bridgman and gradient-freeze techniques that lead to poor control of heat transport during crystallization. The goal of the project was to develop an advanced HP crystal-growth system with flexibility and stability that will allow the growth of CdZnTe ingots (a) without cracking, (b) with higher single-crystal yield, and (c) with improved charge-transport properties reproducibly.

In this paper, we discuss the development of the vertical HP-EDG crystal-growth system and the properties of the large-diameter (140 mm), SI $Cd_{1-x}Zn_xTe$ ($x = 0.1$) ingots grown by the technique. The experimental results confirm the predictions of the computational fluid-dynamics (CFD) model for the dramatic reduction of thermal stress and the elimination of cracking of the ingots grown in moderate temperature gradients. The CdZnTe 10-kg ingots grown by the HP-EDG systems also show increased single-crystal yield and improved electron transport. The increased single-crystal volume is associated with more stable growth conditions throughout the crystallization of the ingot using the EDG technique. The 16 ingots grown to date with the two new HP-EDG systems show electron mobility-lifetime product ($\mu\tau_e$) in the $(2.5–7.5) \times 10^{-3}$ cm^2/V range and display excellent ingot-to-ingot reproducibility.

HP-EDG SYSTEM DEVELOPMENT

Because the main goal of the HP-EDG development project was to improve the control over heat transport in the HP growth system, we chose to employ heat-transport modeling and thermal stress analysis to design the new crystal-growth system. The eV PRODUCTS process development team worked with Cape Simulations Inc.[15] to develop the CFD model of heat and mass transport. The two-dimensional CFD model uses the Fluent CFD package (Lebanon, NH) and describes heat and mass transport in the whole HP chamber including radiative, convective, and conductive transport in the solid, liquid, and gas phases. It predicts the shape of the crystallization interface, convection patterns in the molten CdZnTe, and performs a stress analysis in the solidified CdZnTe ingot. The modeling tool has been installed at eV PRODUCTS to aid further process development and growth-system engineering efforts.

The thermal modeling project was set up in four phases. In the first phase, the CFD model of the HPB/HPGF furnace (Gen-2+) was developed. In the second phase, the validity of the CFD model was evaluated and verified. The transport model, geometry, and material properties were adjusted to describe the experimentally measured temperature distribution in the furnace with satisfactory

accuracy. Once the heat-transport model was experimentally validated for the Gen-2+ HPB/HPGF furnace, in the third phase, the CFD model of the HP-EDG furnace was developed. Finally, in phase four, various growth scenarios were evaluated, and the predicted thermal stress analyzed. Results from the CFD model and stress analysis are discussed later.

Once the thermal model was completed, and the model calculations suggested that the conceptualized system will meet the design goals and will allow the growth of CdZnTe with much reduced thermal stress, the mechanical design of the crystal-growth system was completed. The design and process development retained the 5.5-in. (140 mm) ingot diameter and pressure chamber size. This allowed us to keep some of the mechanical components of the existing Gen-2+ HP systems and, more importantly, will allow faster future upgrades of the Gen-2+ HPB/HPGF systems to the Gen-3 HP-EDG system. The power, control, and data acquisition systems for the new HP-EDG systems also included several upgrades to improve the stability and reliability of the systems. The flexibility of the multi-zone heater system allows dynamic control of heat flow to optimize the growth-interface shape during crystallization. This flexibility combined with an advanced control system, improved system diagnostics, and realistic thermal modeling provides an excellent platform for further process development.

Thermal Model

Figure 1 shows an example of the simulated temperature distribution and melt-flow pattern for CdZnTe growth in the HP-EDG furnace. In this example, about one third of the melt is solidified. The model predicts the existence of convection vortices centered in the proximity of the ampoule wall and the strong flattening of the melt/solid interface because of the strong convective-heat transport. The model also predicts a concave melt/solid interface

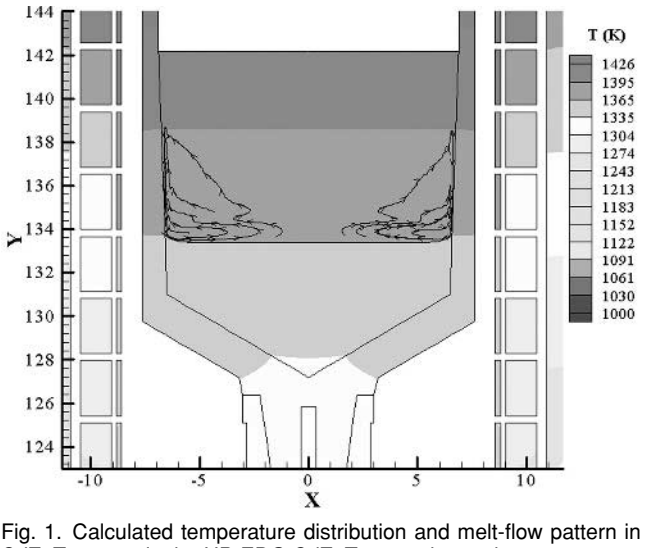

Fig. 1. Calculated temperature distribution and melt-flow pattern in CdZnTe grown in the HP-EDG CdZnTe crystal-growth system.

along the crucible wall. This is a highly undesirable effect as it stimulates parasitic secondary-grain nucleation and growth from the crucible wall and is one of the main hindrances for the growth of large CdZnTe single crystals in the vertical configuration in containers with strong melt-wall interactions. The effect is the direct consequence of the large latent heat of CdZnTe released during solidification at the interface, low thermal conductivity of solid CdZnTe, and the large thermal conductivity of the graphite container. Our further process development will focus on optimizing the growth conditions to obtain a favorable heat-transport pattern in the system and suppressing parasitic secondary-grain growth originating at the crucible wall.

Stress Analysis

Figure 2 compares the calculated temperature distribution and distribution of von Mises stresses for CdZnTe ingots solidified in the Gen-2+ HPB/HPGF and Gen-3 HP-EDG systems. The results confirm the excessive stress in ingots grown in the Gen-2+ HPB/HPGF systems and the 8–10 fold reduction of thermal stress in the HP-EDG system. The maximum stress predicted for the Gen-2+ HPB/HPGF system ($\sim$350 N/cm^2) is well above the critical-resolved stress reported for CdZnTe ($\sim$43 N/cm^2).[16] In the Gen-3 HP-EDG system, the maximum stress ($\sim$38 N/cm^2) is below the critical-resolved stress, so no ingot cracking is expected with the calculated temperature distribution. The model also predicts stress distribution similar to those predicted by others in the literature. More importantly, the model correctly predicts the maximum stress points in the CdZnTe ingots and shows excellent agreement with the cracking pattern observed experimentally. This result provides further confirmation that the model gives a correct description of the heat-transport phenomena in the HP-EDG system.

CRYSTAL-GROWTH RESULTS

Structural Properties

We have performed 16 CdZnTe crystal growths in the two new Gen-3 HP-EDG furnaces to date. Figure 3 shows a typical ingot and axial slices from the ingot. No cracking is observed in these ingots, verifying that the furnaces perform according to the design specifications, and the thermal stress is sufficiently low during crystallization and cool down of the ingot. The axial slice from the CdZnTe ingot shows few large-volume single crystals dominating a large fraction of the slice. Numerous smaller secondary grains are also observed particularly in the first-to-freeze (tip) section and along the periphery of the ingot. This indicates that considerable secondary-grain nucleation takes place along the crucible wall. Some of the grains show twins. Overall, the concentration of twins is lower than in ingots grown by the HPB and HPGF processes. The origin of twinning is not fully understood in CdZnTe, but

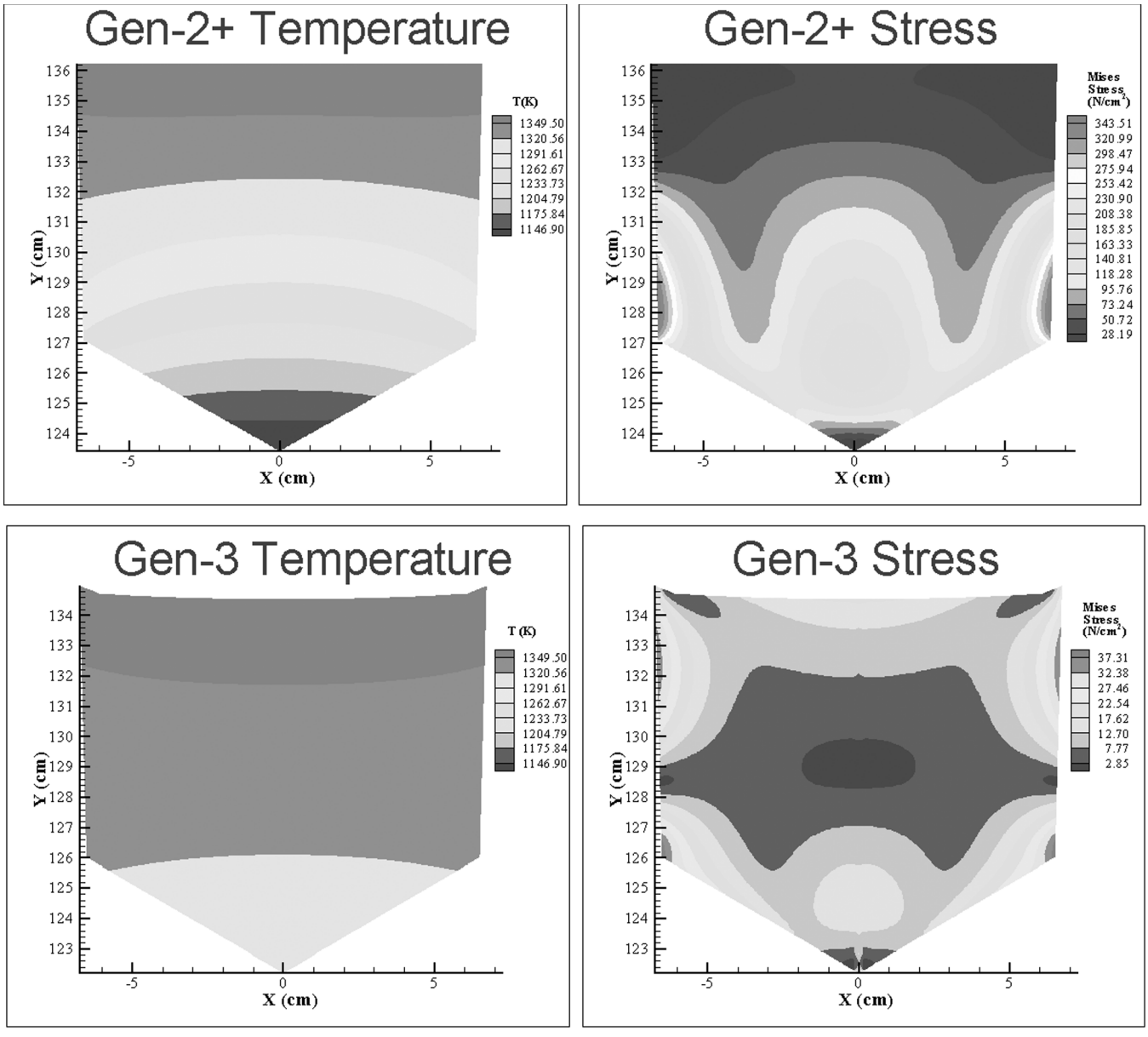

Fig. 2. Temperature distribution (left panes) and von Mises stress distribution (right panes) in the Gen-2+ HPB/HPGF and HP-EDG furnace for completed solidification. Note the factor of 10 higher stress in the HPB/HPGF system. The CFD model predicts high stress points at locations where cracking occurs experimentally.

it is often associated with unstable growth conditions.[17] The observed less twinning correlates well with the improved heat-flow control and more stable growth conditions in the HP-EDG systems.

Figure 4 shows an infrared (IR) microscopy map of an axial slice from the first ingot grown by the HP-EDG furnace. The IR microscopy is a convenient tool to visualize Te inclusions in CdZnTe ingots. Because the inclusions are pure Te phases, they strongly absorb IR light and appear as dark features in the IR images. The formation of Te inclusions is expected, as we chose to grow the ingots from Te-rich melt. It is to be noted here that the Te phases resolved by IR microscopy with diameter $\geq$1 μm are often incorrectly called Te precipitates in the literature. Although Te precipitates form in large concentration during CdZnTe crystallization from Te-rich melt; their average diameter is in the 10–30-nm range and cannot be resolved using IR microscopy. Precipitates originate from the retrograde solubility of Te in CdZnTe and their nucleation and growth is controlled by atomic diffusion and the precipitation process.[18,19] In contrast to precipitates, the typical diameter of Te inclusions is in the 1–50-μm range. The maximum solubility of Te in CdZnTe cannot supply enough excess Te to form such large-size Te agglomerates.[19] Inclusions originate from morphological instabilities at the growth interface, as Te-rich melt droplets are captured from the boundary layer ahead of the interface.[18]

Most of the inclusions seen in Fig. 4 have a triangular- or faceted-polyhedron shape, indicating that

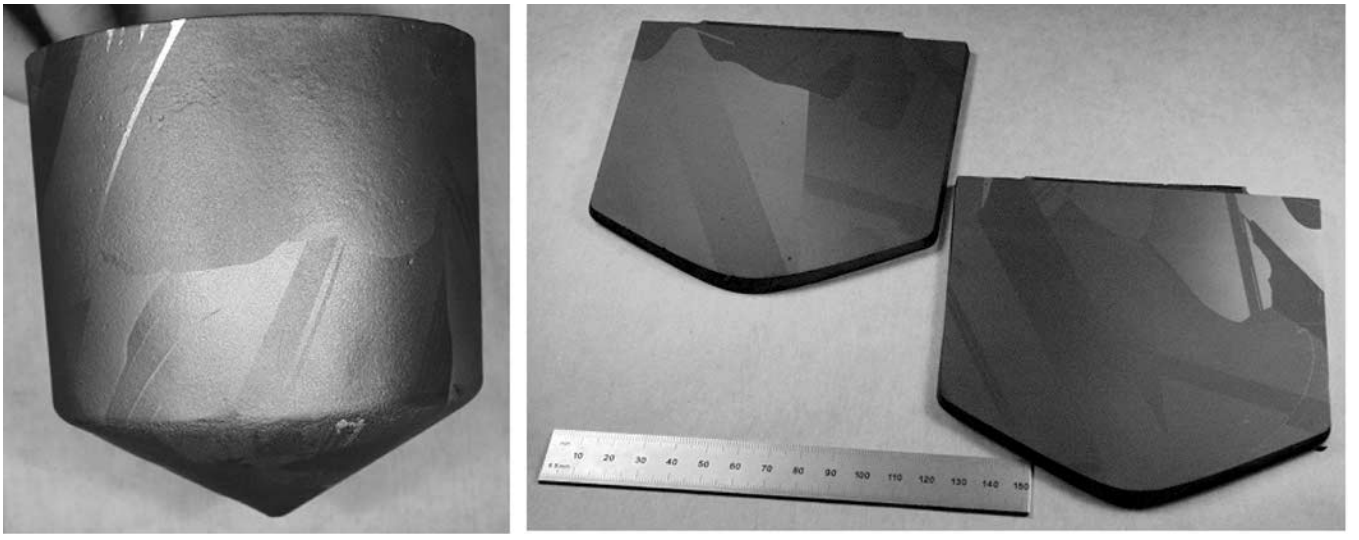

Fig. 3. Typical 5.5-in. (140 mm) diameter, 10-kg CdZnTe ingot grown by the HP-EDG system. Two 5-mm-thick axial slices are also shown.

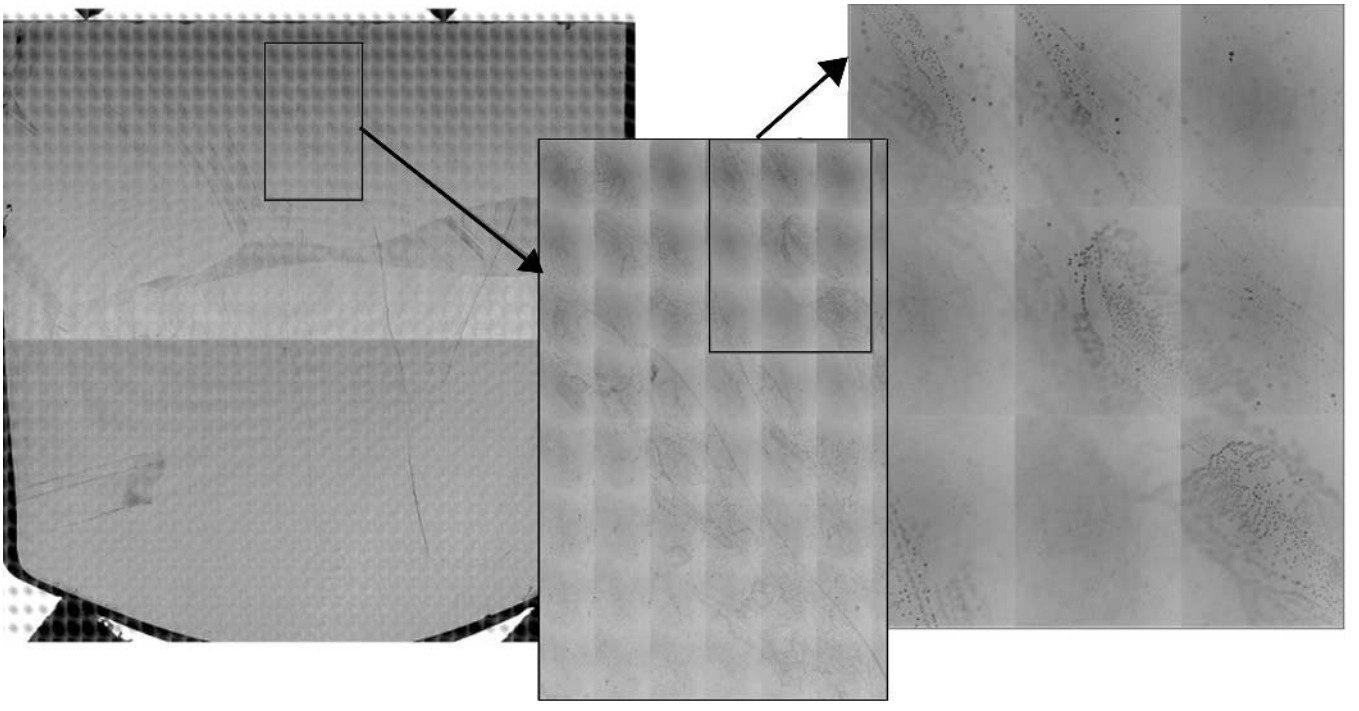

Fig. 4. The IR microscopy map of an axial slice from an early CdZnTe ingot grown by the HP-EDG technique. In the full area map, Te-inclusion-rich areas appear as dark sections. These are typically grain boundaries decorated with Te inclusions. The inset shows a high Te-inclusion density area close to the heel (last-to-freeze) section. Individual inclusions up to 50 μm in diameter are clearly resolved in this image.

they have a well-defined crystallographic orientation relative to the surrounding CdZnTe matrix.[4,20] Figure 5 shows a higher magnification IR image of triangular- and polyhedron-shaped Te inclusions. The Te inclusions have an elongated plate or saucer shape within grain boundaries; but even here, they tend to line up with neighboring grains and form sharp boundaries.[21] There is significant evidence that Te inclusions and the surrounding defect field have a strong detrimental effect on electron transport in CdZnTe crystals and on the poor performance of the fabricated detector devices.[22,23] It was also shown that the region of degraded charge transport near Te inclusions extends well beyond the volume of the inclusions themselves.[23] This might be due to the field of dislocations and Te precipitates surrounding Te inclusions.[4] Recently, it was indeed shown that dislocations cause severe carrier trapping and hamper charge transport in CdZnTe.[24] It is, therefore, reasonable to expect that suppression of the formation of Te inclusions and the defect-field around them will improve carrier transport in CdZnTe crystals and the performance of radiation detector devices fabricated from these crystals.

The two main parameters controlling the formation of Te inclusions are the melt composition and

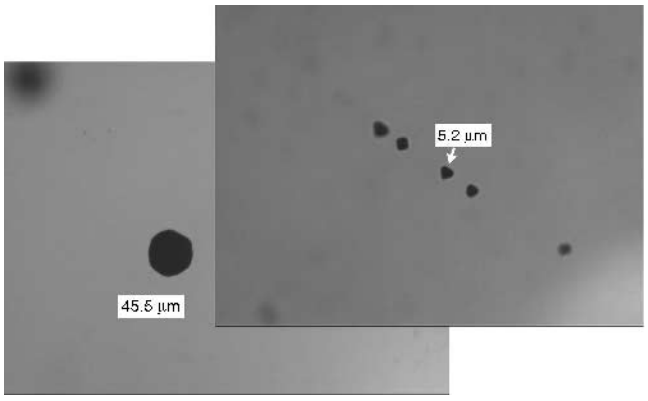

Fig. 5. The IR images of triangular and faceted polyhedron-shaped Te inclusions in the HP-EDG-grown CdZnTe ingots.

the temperature gradient at the solidification interface. Because of the noncongruent nature of CdZnTe solidification from the non-stoichiometric melt, the solid rejects a fraction of the excess Te in the melt, which is gradually enriched in Te as solidification proceeds. In addition, because of the limited mixing of the melt near the solidification interface, a Te-rich boundary layer is formed at the interface. This Te-rich boundary layer provides the supply of the excess Te that is captured at instability locations along the interface. By controlling the melt stoichiometry, the Te enrichment of the boundary layer can be reduced, and the formation of Te inclusions can be suppressed. This can be achieved by passive (load composition) or active (component partial pressure) control of the melt stoichiometry. The growth of virtually Te-inclusion-free SI CdZnTe crystals has been demonstrated with this technique.[4,25] Alternatively, imposing a larger temperature gradient during the growth can also reduce Te-inclusion formation. Indeed, we observe a lower Te-inclusion density in CdZnTe ingots grown using much larger temperature gradients in our older HPB systems.

Charge-Transport Properties

To transport the charge carriers through CdZnTe devices several millimeters or centimeters thick, the mobility (μ) and lifetime (τ) of the carriers has to be sufficiently high to avoid carrier trapping and recombination and the deterioration of the signal pulse amplitude. While the electron mobility (μ_e = 1,000–800 cm^2/Vs) and lifetime (τ_e = (1–5) $\times$ 10^{-6} s) are relatively high, the hole mobility (μ_h = 80–30 cm^2/Vs) and lifetime (τ_e = 10^{-6}–10^{-7} s) are typically very low in CdZnTe. The low hole transport poses a significant problem at high photon energies, where a significant fraction of the photon absorption takes place deep in the device, and a large fraction of the preamplifier voltage pulse is generated by integration of the hole current. In most applications requiring good spectral-resolution, CdZnTe-detector readout schemes that use only (or largely) the electron signal and suppress the hole contribution are used.[26–28] Among these the coplanar-grid (CPG) detector configuration and readout scheme is the most widely used in high-energy spectroscopic applications.[26]

To study the charge-transport properties of the CdZnTe crystals grown by the HP-EDG process, 10 $\times$ 10 $\times$ 2 mm^3 samples were fabricated from radial slices cut close to the first-to-freeze (tip, $\sim$ 0.1 solidified fraction) and last-to-freeze (heel, $\sim$ 0.95 solidified fraction) sections of the ingot. The samples were etched in a dilute Br-methanol solution to remove the surface damage introduced during cutting. Platinum electrodes were deposited by sputtering onto the 10 $\times$ 10 mm^2 area surfaces of the crystals to form detector structures. The bulk electrical resistivity of the material is determined from the low-voltage region of current-voltage measurements. The measured resistivity of the ingots is in the (2–3) $\times$ 10^{10} Ωcm range and shows very little variation between the tip and heel section of the ingots. The measured resistivity variation from tip to heel is less than the one expected from the bandgap variation because of the Zn distribution ($\sim$12% tip and $\sim$6% heel). This suggests that impurity segregation compensates for the bandgap variation. The high measured resistivity indicates that the material is fully compensated throughout the ingot volume (at least within the 0.1–0.95 solidified-fraction region studied).

The mobility-lifetime product ($\mu\tau$) of the charge carriers was determined from the bias dependence of the charge collection efficiency. To evaluate the collection efficiency and estimate the $\mu\tau$ values, the shift of the pulse height of the photo peak from the 5.5-MeV alpha particles from a ^{241} Am source was measured as a function of the bias voltage, and the resulting data fitted to the Hecht equation.[29] Figure 6 shows the experimental setup for $\mu\tau$ measurements. Because the 5.5-MeV alpha particles are fully absorbed within 18 μm of the entrance surface of the samples, essentially, only one type of carrier has to traverse the volume of the device. Depending on the polarity of the applied bias voltage, the charge-transport properties of electrons and holes can be independently studied. With the employment of a collimated alpha source, the technique can be also used to map the charge-transport properties of large-volume CdZnTe crystals.[23]

Figure 7 shows the Hecht curves for electrons obtained on 14 samples from a CdZnTe ingot grown by the HP-EDG process. The average electron mobility-lifetime product was $\mu\tau_e$ = 5.3 $\times$ 10^{-3} cm^2/V for these 14 samples. The Hecht curves and electron mobility-lifetime products show very little variation from sample to sample, indicating that the material is very uniform on a macroscopic scale (microscale variation is discussed later). The hole mobility-lifetime product of the material was estimated to be in the $\mu\tau_h$ $\cong$ (0.2–1) $\times$ 10^{-5} cm^2/V range. For such a low value, it is difficult to reliably measure $\mu\tau_h$ with the current technique. For the 14 ingots grown to date in the two HP-EDG systems, we find $\mu\tau_e$ to vary in the (2.5–7.5)

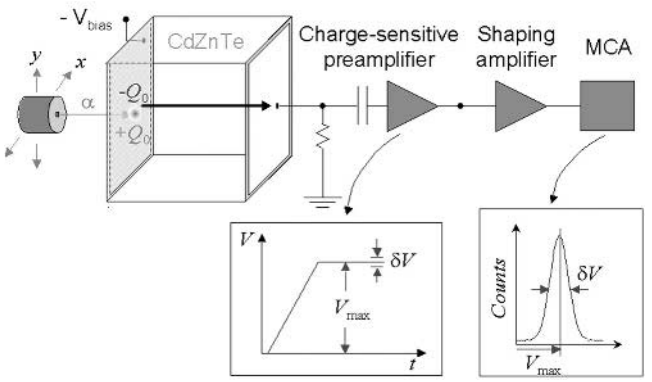

Fig. 6. The principle of charge-transport measurements in CdZnTe crystals using alpha particles. The alpha particles create a cloud of electron-hole pairs close to the entrance electrode. The electrons and holes are separated and move to the opposite electrodes in the electric field. The current is integrated with a charge-sensitive preamplifier to create a voltage pulse. The voltage pulses are amplified and collected as a histogram in a multichannel analyzer. Charge trapping in the device causes a reduction of the voltage pulse amplitude and the shift of the peak to lower channels. Measurement of the peak position (or voltage pulse amplitude) as a function of the bias voltage allows the determination of the mobility-lifetime product of the carriers.

$\times 10^{-3}$ cm^2/V range; however, some ingot sections yield material with $\mu\tau_e \geq 8 \times 10^{-3}$ cm^2/V.

The detector response of 15 × 15 × 7.5 mm^3 crystals from an early CdZnTe ingot grown by the HP-EDG technique is illustrated in Fig. 8. These data were taken in the CPG configuration with bias voltage and differential bias optimized to get the best energy resolution for the 662-keV photo peak from ^{137}Cs. The 3% and 3.5% resolution full width half maximum is worse than expected from the electron mobility-lifetime product and biasing conditions. One possible explanation for the poor energy resolution is the microscopic-scale spatial nonuniformity of the charge transport in the volume of the detectors.[22,23]

Charge-Transport Uniformity

To study the charge-transport uniformity of the SI CdZnTe crystals, we constructed an alpha-particle mapping system.[23] The system is illustrated in Fig. 6. For charge-transport mapping purposes, a collimated ^{241}Am alpha source is placed on an X-Y stage. To avoid the scattering and energy loss of the alpha particles as they travel from the source to the CdZnTe crystal, we placed the alpha source, X-Y stage, sample fixture, and preamplifier in a vacuum chamber. The system currently employs a 1-mm-diameter collimator. The stage control and data acquisition is fully automatic and can do point-by-point μτ measurements in the crystals. Because the alpha particles produce a sharp peak even simple peak position or peak shape analysis can provide excellent assessment of the charge-transport uniformity of the crystals. Figure 9 shows an example of alpha-particle charge-transport mapping. The studied 12 × 12 × 5.4 mm^3 CdZnTe crystal contains significant concentration of Te inclusions, some of which decorate a twin

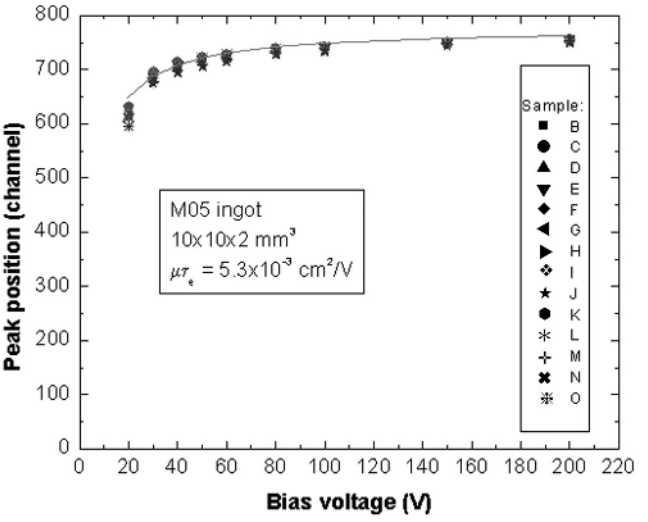

Fig. 7. Peak position versus bias voltage (Hecht curve) for 14 samples from the same CdZnTe ingot grown by the HP-EDG technique. The data show little variation from sample to sample, indicating good charge-transport uniformity in the ingot. The high average $\mu\tau_e = 5.3 \times 10^{-3}$ cm^2/V shows very good electron transport in the material.

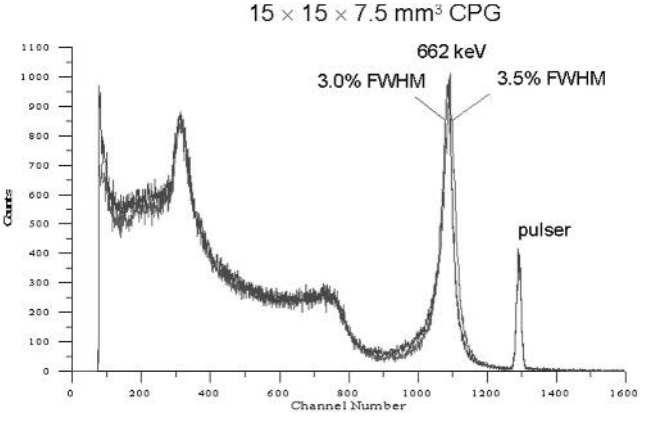

Fig. 8. The detector response of 15 × 15 × 7.5 mm^3 crystals from an early CdZnTe ingot grown by the HP-EDG technique in the CPG configuration to ^{137}Cs radiation.

plane. Because of the trapping of electrons, the alpha-particle spectrum strongly deteriorates in the area of the decorated twin plane. The peak position of the alpha spectrum shifts to a lower channel, and a low energy tail distorts the spectrum. In other sections of the crystal, away from the decorated twin plane where only randomly distributed Te inclusions are visible in the IR image, the alpha spectrum has a more ideal, symmetrical shape and is positioned at a higher channel number. This shows much less trapping in this area of the crystal.

In large-volume CdZnTe detectors, the signals from various parts of the crystal are collected, and the resulting cumulative gamma-ray spectrum reflects the spatial charge-transport uniformity of the crystal. Alpha-particle mapping studies confirmed that charge-transport nonuniformity, similar to that observed for the CdZnTe crystal in Fig. 9, is responsible for the poor performance of the CPG detectors in Fig. 8. Our combined IR and alpha-particle mapping

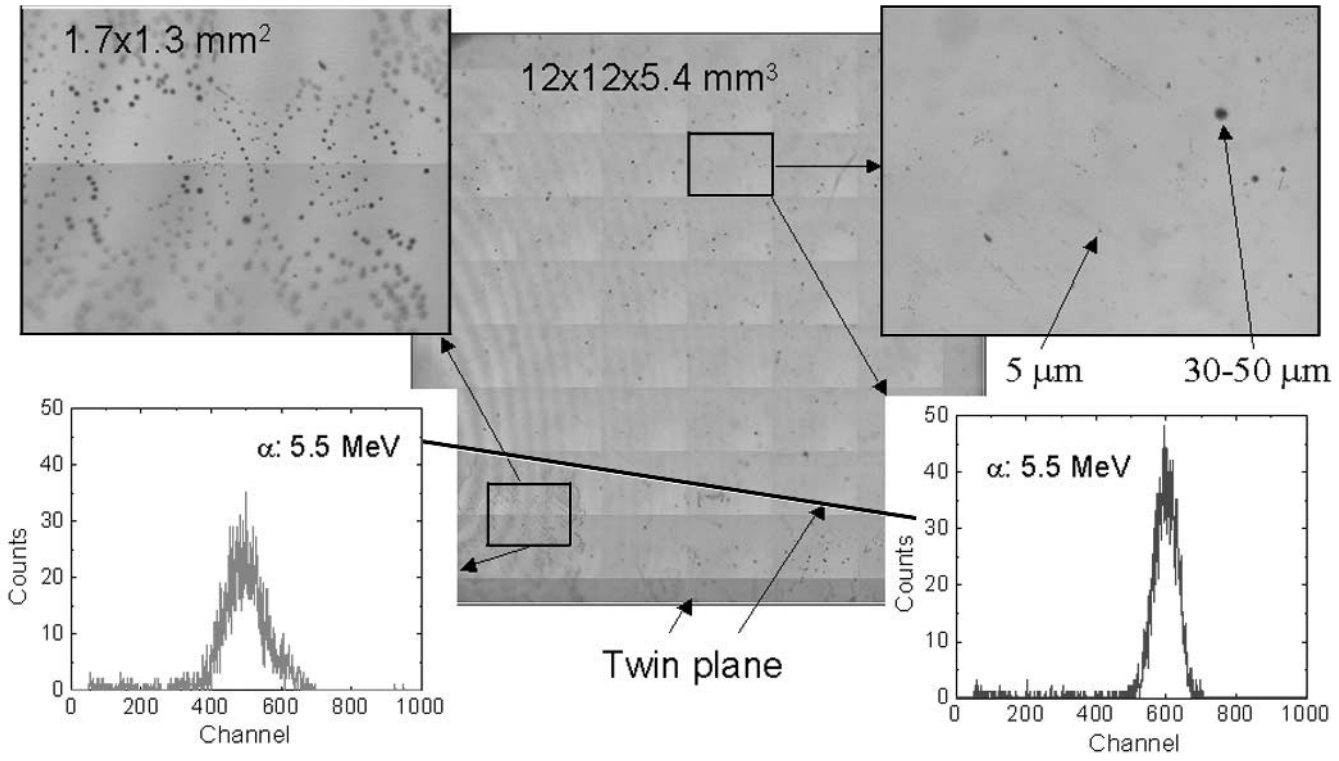

Fig. 9. Alpha-particle mapping of a 12 × 12 × 5.4 mm^3 CdZnTe crystal. The IR mapping reveals large Te inclusions, in a twin plane in the crystal. Strong deterioration of the alpha spectrum is found in the area of the decorated twin plane.

results so far support previous observations that correlated clusters of large-size Te inclusions deteriorate charge-transport uniformity in CdZnTe crystals.[22,23] It is anticipated, therefore, that, by suppressing Te-inclusion formation in the CdZnTe ingots, the microscopic-scale charge-transport nonuniformity can be reduced, and the energy resolution of these devices can be significantly improved.

We continue our crystal-growth process development experiments in an attempt to suppress Te-inclusion formation in SI CdZnTe ingots. Because Cd loss from the crucible cannot be completely eliminated in the current version of our HP-EDG system, we opted to explore the use of somewhat larger temperature gradients to suppress Te-inclusion formation. Figure 10 shows an IR microscopy map of an axial slice from a CdZnTe ingot grown with a nominally larger temperature gradient. Note that only the nominal temperature gradient imposed by the heater can be measured. The actual temperature gradient controlling crystallization is expected to be lower than the imposed gradient and to vary along the growth interface with distance from the ingot axis. Figure 10 shows an overall reduction in the density of Te inclusions. The larger magnification inset shows a single-crystal area with a more dispersed distribution of Te inclusions.

Figure 11 shows the performance of 15 × 15 × 7.5 mm^3 CdZnTe detectors in the CPG device configuration for 662-keV gamma rays. The detector with higher density of Te inclusions shows a rather poor energy resolution of 3.2%. In contrast, the detector employing a CdZnTe crystal grown in a larger temperature gradient and containing a lower density of Te inclusions shows an excellent 2.6% energy resolution. Such a good energy resolution is sufficient for a number of practical applications.

CONCLUSIONS

The HP-EDG crystal-growth technology has been recently developed and introduced at eV PRODUCTS to grow large-volume, SI CdZnTe single crystals for room-temperature x-ray and gamma-ray detector applications. The new HP growth technology significantly improves the downstream CdZnTe device-fabrication yield compared to earlier versions of the HP crystal-growth technology because of the improved structural and charge-transport properties of the CdZnTe ingots. The new state-of-the-art, HP-EDG crystal-growth systems offer exceptional flexibility and thermal and mechanical stability and allow the growth of high-purity CdZnTe ingots. This flexibility combined with an advanced control system, improved system diagnostics, and realistic heat-transport modeling provides an excellent platform for continuing process development. Initial results on large-diameter (140 mm), SI $Cd_{1-x}Zn_xTe$ (x = 0.1) ingots grown in low temperature gradients with the HP-EDG technique show reduced defect density and complete elimination of ingot cracking. The increased single-crystal yield combined with the improved charge transport allows the fabrication of large-volume, high-sensitivity, high energy-resolution detector devices at increased yield. The CdZnTe ingots

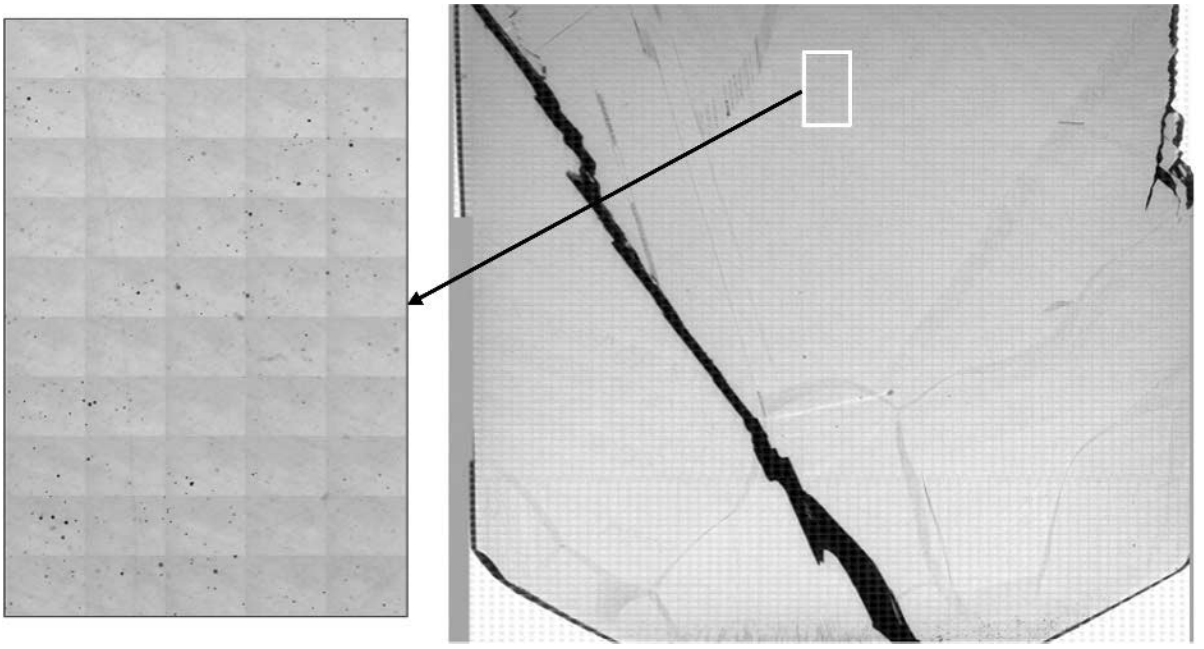

Fig. 10. The IR microscopy map of an axial slice from a CdZnTe ingot grown by the HP-EDG technique with larger temperature gradient. In the full area map, Te-inclusion-rich areas appear as dark sections. These are typically grain boundaries decorated with Te inclusions. The inset shows an area close to the heel (last-to-freeze) section of the ingot containing randomly dispersed Te inclusions. Individual inclusions up to 50 μm in diameter are visible in this image. The diagonal crack occurred during cutting the slice.

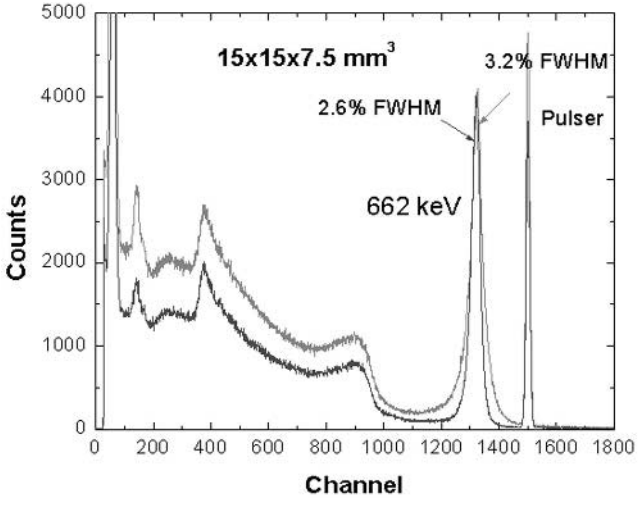

Fig. 11. The detector response of 15 × 15 × 7.5 mm^3 crystals from CdZnTe grown by the HP-EDG technique in the CPG configuration to ^{137}Cs radiation. The CdZnTe crystal for the 2.6% energy-resolution detector was grown in a larger temperature gradient and contains a lower concentration of Te inclusions.

grown to date produced large-volume crystals (≥1 cm^3) with electron mobility-lifetime product ($\mu\tau_e$) in the (3–7) × 10^{-3} cm^2/V range. The lower-than-desired charge-transport uniformity of the HP-EDG CdZnTe ingots is associated with the high density of Te inclusions formed in the ingots during crystallization. The latest process-development efforts show a reduction in the Te-inclusion density, an increase of the charge-transport uniformity, and improved energy resolution of the large-volume detectors fabricated from these crystals.

ACKNOWLEDGEMENTS

The authors are indebted to P.N. Luke (LBL), M. Amman (LBL), and S. Motakef (Cape Simulations) for many useful discussions.

REFERENCES

1. R.B. James, T.E. Schlesinger, J. Lund, and M. Schieber, *Semiconductors and Semimetals*, Vol. 43 (Academic Press, New York, 1997), pp. 335–381.
2. K.B. Parnham, *Nucl. Instr. Meth.* A377, 487 (1996).
3. T.E. Schlesinger, J.E. Toney, H. Yoon, E.Y. Lee, B.A. Brunett, L. Franks, and R.B. James, *Mater. Sci. Eng.* R32, 103 (2001).
4. C. Szeles, W.C. Chalmers, S.C. Cameron, J.-O. Ndap, M. Bliss, and K.G. Lynn, *Proc. SPIE* 4507, 57 (2001).
5. M. Fiederle, V. Babentsov, J. Franc, A. Fauler, and J.-P. Konrath, *Cryst. Res. Technol.* 38, 588 (2003).
6. E. Raiskin and J.F. Butler, *IEEE Trans. Nucl. Sci.* NS-35, 81 (1988).
7. F.P. Doty, J.F. Butler, J.F. Schetzina, and K.A. Bowers, *J. Vac. Sci. Technol. B* 10, 1418 (1992).
8. C. Szeles and E.E. Eissler, *MRS Symp. Proc.* 487, 3 (1998).
9. Saint-Gobain Crystals and Detectors (formerly Bicron), Solon, OH.
10. Imarad Imaging Systems, Israel. See also T.E. Schlesinger et al., *J. Electron. Mater.* 28, 864 (1999).
11. Acrorad, Okinawa, Japan and Eurorad, Strasbourg, France.
12. Yinnel Tech, South Bend. IN. See also L. Li et al., *Proc.* SPIE 4784, 76 (2003).
13. Fermionics Corp., Simi Valley, CA. See also M. Chu, S. Terterian, D. Ting, R.B. James, M. Szawlowski, and G.J. Visser, *Proc. SPIE* 4784, 237 (2003).
14. J.M. Parsey, Jr. and F.A Thiel, *J. Cryst. Growth* 73, 211 (1985).
15. Cape Simulations, Newton, MA, www.capesim.com
16. C. Parfeniuk, F. Weinberg, I.V. Samarasekara, C. Schvezov, and L. Li, *J. Cryst. Growth* 119, 261 (1992).
17. P. Rudolph, *Progr. Cryst. Growth Characterization* 29, 275 (1994).

18. P. Rudolph and M. Mühlberg, *Mater. Sci. Eng.* B16, 8 (1993).
19. J.H. Greenberg, V.N. Guskov, V.B. Lazarev, and O.V. Shebershneva, *J. Solid State Chem.* 102, 382 (1993).
20. J. Shen, D.K. Aidun, L. Regel, and W.R. Wilcox, *J. Cryst. Growth* 132, 250 (1993).
21. J.R. Heffelfinger, D.L. Medlin, and R.B. James, *MRS Symp. Proc.* 487, 33 (1997).
22. M. Amman, J.S. Lee, and P.N. Luke, *Proc. SPIE* 4507, 1 (2001).
23. M. Amman, J.S. Lee, and P.N. Luke, *J. Appl. Phys.* 92, 3198 (2002).
24. N. Krsmanovic, K.G. Lynn, M.H. Weber, R. Tjossem, S.A. Awadalla, C. Szeles, J.P. Flint, and H.L. Glass, *Proc. SPIE*. 4141, 219 (2000).
25. C. Szeles, S.C. Cameron, J.-O. Ndap, and W.C. Chalmers, *IEEE Trans Nucl. Sci.* 49, 2535 (2002).
26. P.N. Luke, *Appl. Phys. Lett.* 65, 2884 (1994).
27. H.H. Barrett, J.D. Eskin, and H.B. Barber, *Phys. Rev. Lett.* 75, 156 (1995).
28. A. Shor, Y. Eisen, and I. Mardor, *Nucl. Instr. Meth. A* 428, 182 (1999).
29. K. Hecht, *Z. Phys.* 77, 235 (1932).